



Review

A Review of Non-Destructive Techniques for Lithium-Ion Battery Performance Analysis

Ximena Carolina Acaró Chacón Stefano Laureti Marco Ricci and Gregorio Cappuccino *

Department of Informatics, Modelling, Electronics and Systems Engineering, University of Calabria, 87036 Arcavacata, Italy; carolina.acaro@dimes.unical.it (X.C.A.C.); stefano.laureti@unical.it (S.L.); marco.ricci@unical.it (M.R.)

* Correspondence: gregorio.cappuccino@unical.it

Abstract: Lithium-ion batteries are considered the most suitable option for powering electric vehicles in modern transportation systems due to their high energy density, high energy efficiency, long cycle life, and low weight. Nonetheless, several safety concerns and their tendency to lose charge over time demand methods capable of determining their state of health accurately, as well as estimating a range of relevant parameters in order to ensure their safe and efficient use. In this framework, non-destructive inspection methods play a fundamental role in assessing the condition of lithium-ion batteries, allowing for their thorough examination without causing any damage. This aspect is particularly crucial when batteries are exploited in critical applications and when evaluating the potential second life usage of the cells. This review explores various non-destructive methods for evaluating lithium batteries, i.e., electrochemical impedance spectroscopy, infrared thermography, X-ray computed tomography and ultrasonic testing, considers and compares several aspects such as sensitivity, flexibility, accuracy, complexity, industrial applicability, and cost. Hence, this work aims at providing academic and industrial professionals with a tool for choosing the most appropriate methodology for a given application.

Keywords: non-destructive testing; non-destructive evaluation; lithium battery; experimental setup; state-of-health; second life usage; electrochemical impedance spectroscopy; infrared thermography; X-ray computed tomography; ultrasonic testing; electric vehicles; safety concerns



Citation: Chacón, X.C.A.; Laureti, S.; Ricci, M.; Cappuccino, G. A Review of Non-Destructive Techniques for Lithium-Ion Battery Performance Analysis. *World Electr. Veh. J.* **2023**, *14*, 305. <https://doi.org/10.3390/wevj14110305>

Academic Editor: Hong Zhao

Received: 8 September 2023

Revised: 28 October 2023

Accepted: 1 November 2023

Published: 3 November 2023



Copyright: © 2023 by the authors. Licensee MDPI, Basel, Switzerland. This article is an open access article distributed under the terms and conditions of the Creative Commons Attribution (CC BY) license (<https://creativecommons.org/licenses/by/4.0/>).

1. Introduction

Batteries have revolutionized industries in several ways, radically changing electronics by enabling portability and mobility, i.e., making medical devices, GPS systems, and remote sensor technologies more accessible and versatile. Aside from consumer applications, batteries play a fundamental role in the energy storage and electric vehicle (EVs) industries. In these applications, secondary batteries can contribute significantly to decarbonization as they can be used for smoothing the fluctuations of renewables, and for the development of more and more accessible and high-performing transport media at zero carbon emissions.

Although other technologies exist for energy storage applications [1], Lithium-ion batteries (LIBs) have become the predominant technology thanks to a good trade-off between fast-charging capability and higher cycle life and energy density compared with other commercially available mature technologies [2–6].

Despite their numerous advantages, the safety and durability of LIBs must be considered carefully. The first challenge is the development of fast and accurate detection technologies for defects that emerge during production, such as surface defects and defects in the electrode plates that might affect the safety and performance of the batteries. Surface defects are mainly caused by damage to raw materials or accidental bumps. Defects in the electrode plates play a detrimental role in battery capacity and service life, often resulting in internal battery malfunction. Potential short circuit and pole piece defect detection must be monitored and identified as well [7].

During LIBs ordinary operation, safety concerns are related to the possibility of overheating and, in extreme cases, to the risk of fire or explosion [8]. Hence, it is crucial to implement proper safety measures in the design, manufacturing, and in the second life of LIBs, through a proper design of thermal management systems or short circuit protection [9,10]. Regarding their durability, LIBs can face degradation over time due to repeated charge–discharge cycles. This might affect their charge retention capacity and their lifespan. Hence, ongoing research is being conducted to improve these aspects through advancements in materials, electrode design, and battery management systems. LIB development focuses on improving their efficiency by using environmentally friendly materials [11].

During the life cycle, batteries can fail due to various factors such as manufacturing errors, abuse conditions, or degradation. Tests have been developed to simulate the mechanical and thermal abuse loads that batteries might encounter during their use [12,13]. New methods are currently being employed in the EV industry that allow for constant monitoring of battery conditions.

From the above discussion it turns out that the faithful estimation of LIBs' global state of health (SOH) is crucial for guaranteeing effective battery management and a safe and reliable operation. Moreover, SOH should be estimated without damaging or triggering future failures of the battery, hence the need for non-destructive testing (NDT) techniques [14–16].

NDT refers to a range of methods for evaluating and localizing anomalies such as imperfections, corrosion, deformation, discontinuities, external and internal cracks, etc., during the production and life cycles of LIBs, without compromising the original part, in accordance with the applicable standards [17–19]. In recent years, significant steps have been made in the development of accurate, non-invasive, and reliable methods for the estimation of battery performance. One of the diagnostic tools to assess a battery's state and determine if it is operating optimally or if it requires maintenance or replacement is based on the evaluation of micro-health parameters [20].

The NDT of LIBs can be classified into several categories. The commonly accepted taxonomy is based on their underlying physical principle of measurement, e.g., electromagnetic waves, thermal waves, mechanical waves, etc.

In this article we will discuss the primary NDT techniques employed for LIB monitoring and evaluation, these being electrochemical impedance spectroscopy (EIS), infrared thermography (IRT), X-ray computed tomography (XCT), and ultrasonic testing (UT). EIS can provide important information on the LIBs' electrical properties and can be combined with imaging or data-driven methods to gather a comprehensive view on a battery's SOH. IRT results in a visual representation of the temperature distribution, allowing for quick qualitative analysis and identification of anomalies or defects. UT has become more popular in recent years for the evaluation of SOC and SOH in LIBs and can provide accurate thickness measurements and characterization of material properties.

The objective of this research is twofold. First, the aim is to review the existing NDT methods and measurement schemes for examining batteries, providing the reader with a view on the basic experimental setup for each technique. Secondly, this work aims at aiding in choosing the most suitable measurements techniques, considering recent findings and the required methodology, as well as common issues faced. The sensitivity, the estimation parameters, and the complexity of the experimental setups are some of the aspects examined in the following analysis.

2. Electromechanical Impedance Spectroscopy (EIS)

EIS is based on the measurement of the battery impedance over a range of frequency values. Impedance is a measure of the opposition of a battery over the electrical current flow as a function of the input frequency, i.e., it is the AC counterpart of the resistance in a DC circuit. EIS is used to estimate several battery parameters that are related to the SOC, such as internal resistance, capacity, and time constant [21,22]. The remarkable aspect of

EIS is the ability to provide insight into both the intrinsic characteristics and the surface properties of a system, leveraging parallels to circuit elements.

Figure 1 shows a basic experimental setup for the EIS test, which makes use of an impedance analyzer connected to the electrodes and excites them via an AC voltage/current input in a range of frequency values. In general, a four-electrode cell is used, but in practical applications on commercial cells, a two-electrode configuration is the only one that can be employed, although this leads to a less-precise control of the potential across the electrochemical interface of the cell [23,24].

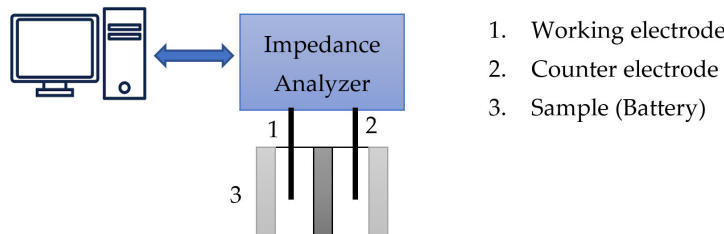


Figure 1. Typical representation of electrochemical impedance spectroscopy (EIS) measurements of a LIB presented in a test setup.

According to the systems theory, the LIB is here considered to be a black box and the response to AC potential or current signals is retrieved over a range of frequencies. The value of the impedance is computed from the mentioned system's output over a set of frequency values, thus resulting in a spectroscopy method. Practically speaking, this means that the diffusion coefficients, kinetic parameters, and electrolyte resistance of the LIB can be retrieved using a single measurement. The impedance is calculated according to Equations (1) and (2). Equation (3) shows how the imaginary (reactance) and real (resistance) parts of the impedance can be used to compute the phase angle, from which meaningful parameters can be inferred. The values of both the resistance and the reactance can also be plotted against each other, i.e., the so-called Nyquist plot, and this can provide further information about the LIB.

In Equations (1)–(3), V_t stands for the potential as a function of time t , I_t is the current, \hat{V} the amplitude of voltage, \hat{I} the amplitude of current, ϕ is the phase shift, Z_0 is the magnitude of impedance, and Z' and Z'' the reactance and resistance, respectively.

As a final remark, note also that galvanostatic EIS is frequently applied to LIBs as well [25].

$$Z = \frac{V_t}{I_t} = \frac{\hat{V}\sin(wt)}{\hat{I}\sin(wt + \phi)} = Z_0 \frac{\sin(wt)}{\sin(wt + \phi)} \quad (1)$$

$$Z_0 = \sqrt{(Z')^2 + (Z'')^2} \quad (2)$$

$$\tan(\phi) = \frac{Z'}{Z''} \quad (3)$$

It must be stressed that EIS data can be used to infer and/or select suitable equivalent circuit models (ECMs) to switch between the mentioned black box approach with a large number of free parameters to smaller, more interpretable, yet controllable, ones. The choice of a given ECM model to describe the behavior of LIBs is not an easy task and it depends on several factors, such as the dynamic range, working conditions, and the battery type (LiPo, LiFePO₄, etc.), as they have different electrochemical characteristics and impedance behaviors, performance at low and high frequencies, the electrochemical components such as electrodes, electrolytes, and separators, the specific application, and eventually, the accuracy to be reached [26,27]. In the framework of battery research and development, highly accurate modelling is sought, while in other processes such as control applications, a

simplified representation may be sufficient. To establish accurate circuit models, a range of proper electrical components, e.g., capacitors, resistors, inductors, and diodes, representing the overall system should be used. In Figure 2, we present an example provided by [28] of ECM that can be used to model a LIB, which is based on the most elementary half-cell system. In the shown model, EIS is used to retrieve the following parameters:

- R_b corresponds to the internal resistance of the bulk materials. When a battery is cycled, the electrolyte is gradually depleted, and microcracks may form within the electrode materials. A decrease in SOH is typically associated with an increase in R_b ;
- R_{SEI} and CPE_{SEI} are the resistance and capacitance of the solid electrolyte interphase layer;
- W is the Warburg impedance and it is related to the diffusion of ions;
- R_{ct} is the transfer resistance, related to the electrochemical reaction kinetics, which change based on the surface coating, phase transition, band gap structure, and particle sizes. R_{ct} is found to be correlated with SOC changes.

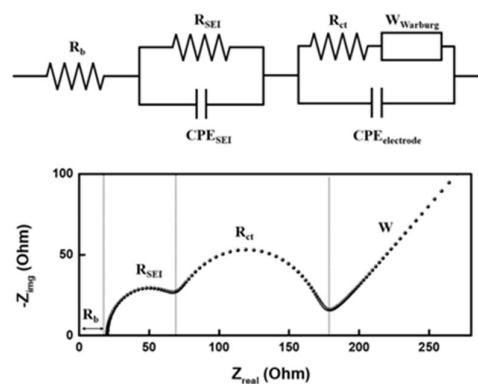


Figure 2. Nyquist plot for a ECM of a LIB half-cell system. Reprinted from [28]—Copyright © 2023 by The Korean Electrochemical Society—CC BY-NC 4.0.

Furthermore, the Nyquist plots depicted in Figure 2, taken from the same work examined above, can exhibit abrupt variations in their trends due to temperature changes. For instance, higher temperatures might result in more pronounced semicircles or shifts in impedance values, so that these can be related to alterations in the battery's electrochemical behavior.

It is important to note that there is no ECM that can be adapted to all types of batteries, though it can be customized depending on the characteristics and specific applications [29–31]. As a matter of fact, according to the properties of the electrochemical cell, a customized circuit model can be created by incorporating or excluding electrical components from an existing one. This is just a snapshot, but it gives an insight into the importance of choosing appropriate ECMs and the difficulties related to such a decision. Once an ECM has been selected and an EIS conducted, it is possible to evaluate fundamental properties that are crucial for understanding and optimizing the performance of batteries through data modelling and parameter analysis.

Related Works

In [25,32], the authors provided an overview of strategies for battery temperature estimation based on EIS. These strategies involve direct phase shift and intercept frequency measurements. To establish the effectiveness of these EIS-based techniques, the authors ran a comparative analysis with other existing apparatus and methods such as temperature sensors, equivalent circuits, and numerical models. Their findings demonstrated that the EIS response profiles are faster in detecting temperature peaks occurring within the LIB compared to conventional temperature measurements.

Furthermore, a study [28] presented a review of how to construct a physically sound circuit model according to the characteristics of the battery system. By establishing a precise circuit model and constructing a uniform cell system to perform an EIS analysis, crucial information about each LIB's component can be obtained. EIS can separate and quantify

the R_b , R_{SEI} , R_{ct} and W by a single experiment, and this can be used to analyze the battery characteristics regarding the state of charge (SOC), temperature, and SOH. EIS can be used to identify highly sensitive parameters (Ohmic resistance, capacitance of the SEI film, charge conduction resistance, and others) that are related to a change in the SOH.

In [33], the authors proposed a time-domain EIS measurement technique followed by an equivalent circuit model interpretation. One of the difficulties in modelling is the choice of initial values, which often makes numerical convergence unachievable if these are wrongly set. The authors of [27] proposed a method to determine and optimize suitable parameters for battery analysis. The method was tested by applying it to two different kinds of LIBs: a lithium iron phosphate (LFP) battery and a lithium cobalt oxide (LCO) one. The proposed method combines several criteria to select a set of suitable values for each parameter, and then employs a quantitative criterion, the so-called Kramers–Kronig relations, to select an optimal parameter value among them. The proposed algorithm is computationally light, and it has been demonstrated that it helps provide meaningful information when used to interpret experimental EIS data.

Recent works make use of ECM and machine learning, including artificial (ANNs) or recurrent neural networks. In particular, machine learning methods have been utilized to enhance the precision and effectiveness of EIS data, enabling the analysis of large datasets of measurements and the creation of predictive models for electrochemical systems. A model for high energy density that uses impedance spectroscopy measurements to monitor the SOH with ANNs has been proposed in [34], and it is based on an equivalent circuit approach. This phenomena is considered important and occurs inside the cell and the subsequent non-linearity of some parameters. In [35], two models for SOH estimation were proposed: one uses a convolution neural network (CNN) to process EIS data, while the other employs a bidirectional long short-term memory (BiLSTM) model for serial regression prediction. Additionally, the authors of [36] established the mapping relationship between health features and SOH using a BP neural network algorithm.

Table 1 provides a summary regarding the primary studies focusing on the prediction of SOC and SOH using EIS. As discussed above, these studies encompass the utilization of two main methodologies: ECMs and machine learning techniques (MLTs). In the case of ECMs, it is possible to obtain important values from each component in a lithium-ion cell via a single experiment. If a circuit model is established with due care and a uniform cell system is constructed to perform an EIS analysis, crucial information about each component of the LIB can be obtained. The experimental measurements can be carried out easily regardless of the battery's state and size. The MLT approach is instead useful when the underlying physical models are not known and/or when the analyzed LIB's systems are rather complex. The effectiveness of MLTs depends largely on the quality of the data, on the appropriate choice of algorithm, and on the correct interpretation of the results. As shown in Table 1, several studies try to combine both the approaches, i.e., the ECMs and MLTs, to speed up the process and reduce the amount of error, leading to more robust and interpretable results with respect to their standalone usage.

To sum up, the EIS data is often analyzed using mathematical models, signal processing techniques, and statistical algorithms to extract the relevant features and patterns associated with the condition of the material. These characteristics can be used to identify and characterize different types of defects, and to estimate their severity and monitor their progression over time. The choice between using a real circuit or a simplified model depends on several factors, including the precision of experimental data, the level of detail required, the complexity of the system, and the objectives of the analysis. In general, detailed information and a deep understanding of the system are sought, hence the need to employ complex models. However, if a faster analysis is needed or detailed data is lacking, employing a simplified model might be a suitable, yet forced choice. In any case, it is important to keep in mind the limitations of any approach.

In conclusion, EIS is a method that in combination with data-driven techniques can achieve high accuracy and it is commonly used for battery characterization and moni-

toring in the automotive and energy storage industries. It can be used to evaluate the electrochemical properties, SOC, SOH, and battery performance. EIS helps in identifying degradation mechanisms, tracking aging effects, and to optimize battery management strategies. Based on the various studies and works analyzed here, this NDT technique is a cost-effective solution in various industrial applications. The cost to arrange an EIS setup can vary depending on the specific requirements, the desired accuracy, and the frequency range of interest, but is in general relatively low.

Table 1. Studies on predicting SOH based on EIS.

Refs.	Parameter	Error (%)	Battery Type	Experimental Setup	Characteristics
[25]	T	<1	Pouch	Abin Battery Cycler Potentiostat: Gamry Interface 5000P, Pennsylvania, USA MZTC Arbin climate-controlled	LCO Li-polymer. Real-time estimator. Online acquisition of impedance ECM was used to interpret and analyze the impedance data at each temperature. Sensitivity to temperature. Low sensitivity to SOC and SOH. ECM: $R_o - (CPE_1 // (R_{ct} - W))$
[34]	SOH	<1	Pouch	Electrochemical Workstation (unreported)	Electrode: LiMnNiCoO ₂ LiPF ₆ Recurrent neural networks (RNNs). Model for high energy density dedicated to EVs. ECM: $R_1 - (R_{2(SOC)} // CPE_1) - CPE_2 - E_{(SOC)}$
[35]	SOH	~5	Coin	Electrochemical Workstation(unreported)	Eunicell LR2032. Five different ECMS. Data-driven algorithm with CNN. ECM and IPSO-CNN-BiLSTM ECM: $R_{ohm} - L_s - (R_{SEI} // CPE_1) - (R_{ct} // CPE_2)$
[36]	RUL	<1	Coin	Electrochemical Workstation (unreported)	Eunicell LR2032. LiCoO ₂ /graphit Real-time battery forecasting system. Gaussian process model and ML. Over 20,000 EIS spectra of commercial Li-ion batteries, with different states of health.
[37]	SOH	3.73–8.66	Pouch	Potentiostat: Gamry Series G300 Keithley 2420 Source Meter Opto-isolated relay board (Devantech RLY816)	LiPO Performance under load. Used parameters of ECM to reproduce the discharge curves. ECM: $R_{ohm} - L - (CPE_1 // R_{ct1}) - (CPE_2 // R_{ct2}) - W$
[38]	SOH	2	Cylindrical	Electrochemical Workstation(unreported)	Commercial Li-ion cells ECM 10 kHz–1 MHz at different SOCs, SOHs, and temperatures. ECM based on the physics of the system. A transmission line model: $(L // R_o) - R_c - [C_g // (C_1 // (R_1 + Z_{d1}) - R_e - C_2 // (R_2 + Z_{d2}))]$
[39]	SOH	1.29–4	Cylindrical	Boling BLC-300 (battery test incubator) Solartron analytical 1470E NEWARE BTS-5V6A	Battery model: 18650. Anode: Graphite. Cathode: LiNi _{0.5} C _{0.2} Mn _{0.3} O ₂ Model-based method. ECM: $R_\Omega - L_s - (CPE_1 // R_{SEI}) - (CPE_2 // R_{ct})$
[40]	SOH	<1.36	Coin	Electrochemical Workstation(unreported)	Eunicell LR2032. Elman NN and cuckoo search (CS-Elman). No building of a circuit model, no consideration of the complex electrochemical reaction.
[33]	SOH	<10 before 240 cycles	Cylindrical	Signal generator V/I converter circuit module (DAQ of NI)	UR14500P Type: LiCoO ₂ . TDIS (time-domain EIS) based on FFT SOH is established by using BPNN (back-propagation NN) algorithm. ECM: $[(C_{dlm} // Z_{FDn}) - R_{film}] // C_{film} - R_o - (C_{dip} // Z_{FDp})$

3. Infrared Thermography (IRT)

IRT is extensively used for quality control and process monitoring in a plethora of industrial applications [41]. Infrared cameras rely on the principle of heat transfer through

radiation, and they contain a focal plane array composed of elements capable of capturing the infrared spectrum emitted by the surfaces of the objects. The impinging radiation is converted into digital data, which are then displayed as an image, and are visualized within the visible spectrum in false color [42–44]. Some cameras are calibrated using radiometric references to accurately record and display measurements in specific units. These cameras are endowed with various sensor types and pixel resolutions in order to capture specific infrared wavebands at the needed level of spatial detail.

For the analysis of LIBs, active thermography systems are increasingly used, in particular the pulsed IRT by exploiting flash lamps. In pulsed IRT, the excitation source is the flashlight. The surface of the battery is exposed to a brief, intense heat pulse produced by the flashlight, see Figure 3. If the LIB's internal structure is flawless and relatively homogeneous, the heat diffuses at the same speed throughout a section of it, thus resulting in a homogenous distribution of the LIB surface temperature. A flaw such as a delamination, a vacancy, or the inclusion of a foreign body, affects the heat diffusion locally, resulting in temporal variations or discrepancies of the surface temperature that can be captured by the IR camera. A computer, equipped with real-time image signal processing and analysis, grabs a time sequence of thermal signals (one for each pixel of the camera sensor), revealing the propagation of thermal energy from the surface to the interior of the target and vice versa.

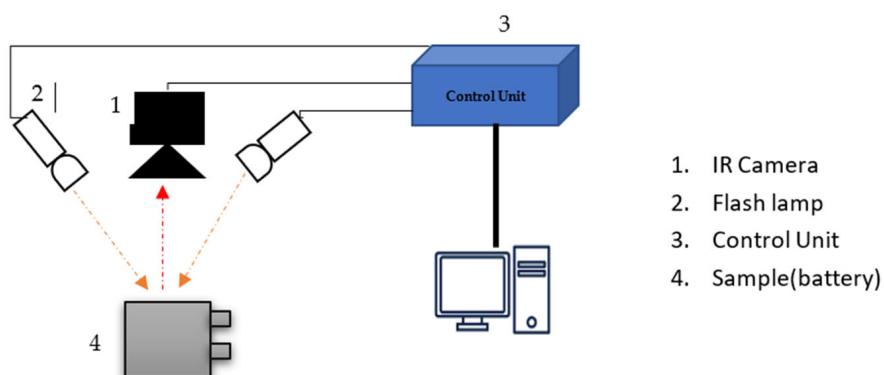


Figure 3. Basic test setup of infrared thermography in reflection mode.

On the other hand, in the passive IRT approach, the heat source is the battery itself. Heat losses within a battery occur from multiple sources, including the entropy change resulting from electrochemical reactions and the Joule's effect, or ohmic heating, caused by current flow across internal resistances and overpotential, see Equation (4). In certain electrochemical combinations, additional electrical energy losses occur, leading to heat generation, for e.g., when attempting to overcharge a fully charged cell.

The first term in Equation (4), represents the heat generation attributed to the reversible entropy change due to the electrochemical reactions within the cell. The second term, accounts for the heat generation resulting from irreversible effects such as ohmic heating and other factors within the cell [45]. Based on these terms and on the discussion above, if the thermal performance of battery pack is not taken into consideration, the rising temperature can cause severe damages to it.

$$q = \left(-I \left[T \left(\frac{dE}{dT} \right) \right] \right) + I(E - V) \quad (4)$$

In Equation (4), q is the heat generation, I the current, T the temperature, the term $\frac{dE}{dT}$ is the temperature coefficient, E the open-circuit potential, and V the cell potential.

Related Works

In [46], an experimental assessment of a commercial LiFePO₄ battery's thermal and electrical performance is reported. The paper highlights that thermal management of LIBs

is a key problem for electric mobility applications, where batteries are subject to severe operating conditions. The comparison between passive IRT and thermo-couple probe measurements showed that the surface temperature was not uniform along the height of the battery, with a greater warming up in its upper zone. In addition to the thermal analysis, the authors also reported an electrical characterization of the LIB, including the cell potential, open circuit potential, and entropic heat coefficient vis à vis the SOC, which were experimentally measured. The obtained experimental data were used to evaluate a simplified heat generation term that is widely employed in numerical approaches.

In [47], the authors discuss the use of pulsed IRT for the inspection of composite material batteries. The article proposes a method for detecting defects in such material using an advanced combination of pulsed thermography and image processing techniques.

In order to foresee the internal heat generation of a lithium-ion pouch cell, the combined use of a lumped capacitance model and thermography is proposed in [48], using a polyimide film heater positioned in front of an IR camera. A series of experiments were carried out to confirm the new method. This method is used to foresee the rate of heat generation in a lithium iron phosphate cell at various discharge rates.

In works [49,50], IRT and thermocouple measurements were used to compare the surface temperatures of lithium-ion polymer cells at various rates of discharge. The experimental measurement aimed at tracking the evolution of the surface temperature of commercial bag cells. The IR images revealed the spatial distribution of the surface temperature, and it was found that the location of the hot spots varies as a function of both the geometrical and material properties of the cell, and according to the type/amount of load applied to the cells.

Various research studies related to thermal analysis and evaluation of different cells are reported in Table 2. The different experimental approaches, methods, and results obtained have been considered in the reported taxonomy. The amount of research performed demonstrates the significance of thermal evaluation in understanding the behavior and performance of batteries. The use of IRT and thermocouple measurements to assess the surface temperature and thermal power estimation seems to be a common approach across the studies. These methods offer valuable insights into the thermal behavior and potential issues of batteries. For instance, the use of pulsed IRT combined with image processing techniques shows promise for defect detection in composite/multi-layer materials. However, when performing pulsed IRT it is important to consider factors such as the difficulty of achieving uniform heating across the battery's surface, as well as thermal conductivity limitations. Additionally, a new non-contact steady-state method for measuring thermal conductivity and thermal contact resistance has been reported [51], providing an alternative approach to evaluating the thermal properties of the battery cell's components.

In summary, IRT is generally used to assess the surface temperature of an LIB, from which information about its internal structure can be inferred such as the presence of gas, pockets or flaws. Active IRT can provide accurate temperature measurements when performed under appropriate conditions, i.e., uniform heating of the inspected surface. When a battery has defects or irregularities on its surface, these areas often have a different thermal conductivity or may be at different temperatures compared to their surroundings, and these can be captured by the thermal camera. IRT can also be used to identify the introduction of contaminating particles, the formation of defects during electrode creation, or to identify holes and a lack of bulk material. The accuracy and sensitivity of the technology depends on the camera quality, calibration, and environmental considerations. While there are a range of options available at different price points, the cost of IRT equipment can vary depending on the desired features and specifications (resolution, spectral sensitivity, or the need for specialized lenses). In most of the research reported here, pouch batteries were tested, demonstrating that the technique is suitable for determining gas pockets and abnormal heat-generation within the battery.

Table 2. Studies on predicting state of LIB based on IRT.

Refs.	Parameter	Error (%)	Battery Type	Experimental Setup	Characteristics
[46]	H-generation	<0.1	Cylindrical	(RMX-4125) programmable power supply (RMX-4005)-DC electronic load NI 6289-data acquisition FLIR SC3000 IR camera thermocouple	Positive and negative electrodes LiFePO ₄ and LiC ₆ . Electrolyte LiPF ₆ . IT and thermocouple probe Increase in the thermal power when the battery is subjected to higher discharge currents. Efficiency decreased with higher C-rates. It describes a heat generation model.
[47]	Thermal abuse	1	Pouch	Li-Polymer battery Infrared camera-FLUKE	LiFePO ₄ The security problem lies in thermal control, including the heat-generation and the internal and external heat transfer.
[48]	H-generation	2.6	Pouch	polyimide film heater FLIR A320-calorimeter	LiFePO ₄ Mathematical model (Biot number, LCM) Lumped capacitance model (LCM) and thermography. Not to be applied where the C-rate is 2C or lower.
[49]	Surface temperature	<10%	Pouch LCO	FLIR E6 thermal imaging camera, thermocouples, humidity sensor black cardboard Applent AT4808 Handheld Multi-channel Temperature Meter	It compares the surface temperature at different discharging rates by infrared thermography and thermocouple measurements. Temperature rises rapidly at higher discharge rates.
[50]	Surface temperature	<1	Pouch NMC, LCO, LPF	NMC-based, LFP, LTO ACT 0550 (80 channels) battery tester (PEC®). NTC 5K thermistor Ti25 thermal imager (FLUKE®)	Evolution of surface temperature. Non-uniformity of the surface temperature.
[51]	Thermal conductivity	12.2	Cilindrical 18650	Coating (XFNANO) laser (MDL-III-808-2W, CNI) Camera (MAG32MINI, Magny).	Negative electrode: Li ₄ Ti ₅ O ₁₂ Non-contact steady-state method. Equivalent thermal circuit.
[52,53]	Defects	1	Coin	FLIR SC-8200 Carl Zeiss Merlin SEM Bruker Nano GmbH using an XFlash 5030 detector Hitachi S3400 SEM	Positive electrode: LiNi _{0.5} Mn _{0.3} Co _{0.2} O ₂ Different plausible defects (agglomeration, blisters, pinholes, metal particle contamination, and non-uniform coating).
[54]	Detection of gas pockets	1	Pouch	PL-565068 infrared camera (FPA InSb FLIRSC5000MB) Potentiostat-IviumStat Current probe-Tektronix A622. Digital acquisition unit-USB 6363 Software-Altair	It demonstrates the effectiveness in the detection of gas pockets formed during cell aging.
[55]	Thermal	1	pouch	ThermaCam-SC640 Fluke 867B multimeter TENMA 72-10505 power supply block TENMA 72-13200 electronic load.	Thermal behavior at different charging and discharging modes.
[56]	H-generation	1	Pouch	Environmental chamber-(Tenney T10c) IR-camera (T650sc, FLIR) T-type thermocoupleSA1-T infrared (IRW-4C, FLIR) Battery tester-BT2000, Arbin Instruments.	Cathode: LiNi _{0.4} Co _{0.2} Mn _{0.2} O ₂ , anode: graphite. Suggesting uniform heating. Hotspot is detected at the activation terminal for improvement of SHLB design. SHLB (self-heating of LIB).
[57]	Cycle Life (RUL)	<10%	pouch	MLX90621-infrared sensor array SUNKEE module ACS712 current sensor. N103-voltage sensors	Combination of infrared thermography and supervised learning techniques. Surface temperature profiles as the input nodes for ANN and SVM models. ANN could estimate the current cycle under 10 min of testing time.

IRT technique can be also combined with other techniques such as the UT, for example for both temperature and SOC estimation [58], as it will be better described in Section 5.

4. X-ray Computer Tomography (XCT)

XCT is used to inspect the internal structure and to gain insight into the mechanical stability limits of the battery components. XCT is an imaging technique that makes use of X-rays to create detailed 3D images of an object's internal structure. It works by taking multiple X-ray images from different angles and leveraging advanced algorithms to reconstruct a 3D image of the object. This technique is widely used in medical imaging to diagnose diseases, injuries, and in other fields such as engineering and materials science to inspect the internal structure of objects without provoking any damage [59,60].

XCT with a resolution on the nanoscale (nano-CT) is extremely desirable for the purpose of characterizing the inner interface [61], i.e., when used to create 3D representations of individual electrodes or the entire cell, and it can output 2D projection images of objects from multiple angles of incidence [62]. It enables the non-destructive inspection of the cell, providing abundant structural information at the micrometer or sub-micrometer levels. This technique can reveal the presence of cracks, voids, and other defects that may affect the performance and safety of the battery. XCT can also be used to study the distribution of active materials in the battery and to monitor changes in its internal structure during charge and discharge cycles. In a recent study, automated registration based on normalized mutual information was applied to align data derived from ultrasonic and radiographic inspections of thin, lithium metal pouch-cell batteries. The quality of the registration was quantified in terms of computational resources and spatial accuracy. In this case, the radiographic data resolution was much higher than the ultrasonic data, and the registration technique was able to align the two datasets accurately. This demonstrates the potential of XCT and other NDT methods to investigate oversized objects such as complete vehicles [63], providing an analysis related to the presence of defects on different automotive components. In addition, it is shown that XCT can provide info about the quality and assembly of components, as well as joining techniques such as welded, adhesive bonded, and sealed connections.

In the electrical vehicle industry, XCT can be used to analyze the internal state of the magnet wires that are needed to meet rigorous usage requirements including heat-resistance property, excellent workability, and insulation properties [64].

In the field of battery research, it is used to study the internal structure of LIBs [65]. Recently, researchers have developed a phosphate solid-state LIB prototype, in which the volume changes during charge and discharge in the materials are minimal according to the theory [3,66]. To understand and optimize the solid-state battery's systems, researchers studied organic–inorganic composite electrolytes and sintered ceramic electrolytes to gain information on the mechanical stability limits [67,68] using XCT. Figure 4 depicts a basic scheme of the method for XCT.

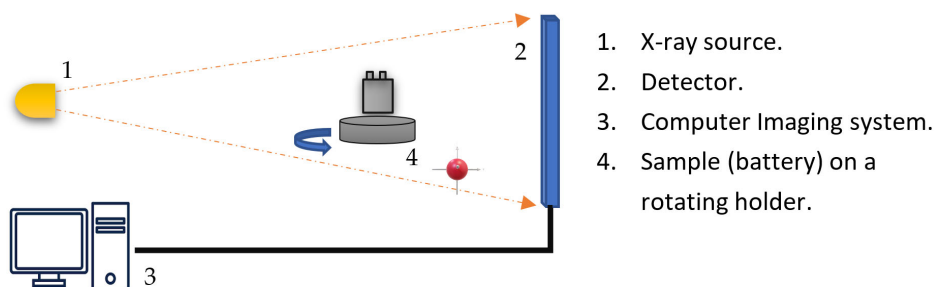


Figure 4. A sketch of a general XCT setup.

Related Works

Table 3 summarizes the most recent studies about XCT and provides valuable insights into the fundamental mechanisms and performance factors of LIBs, contributing to the advancement of battery technology. For instance, in [69] XCT was used to analyze commercial battery materials. The authors gave a guideline to select the imaging equipment and parameters for LIB investigations. The work [70] focused on understanding the capacity detection of lithium-ion based EVs, combined the battery's electrochemical and tomographic

techniques to measure the electrochemical properties and structural parameters of the active materials of the batteries. For cylindrical (18650) cells, welding burrs were noticed on the negative tab of both exploded and fresh cells. Also, three kinds of defects were found for fresh pouch cells, including foreign particles, the overlapping of two electrodes, and structural deformations caused by manufacturing.

In [71], the authors used XCT to investigate the phenomenon of lithium plating in LIBs, the formation and growth of lithium metal deposits on the anode, which can lead to capacity loss, reduced cycle life, and safety issues. In [62], observations and measurements of the sources and progression of electrochemical and mechanical degradation were carried out while batteries were in operation. The model revealed distributions in the initiation and rate of core–shell lithiation, as well as the initiation and growth of cracks along pre-existing defects. Also, the work [72] focused on the non-destructive 3D imaging of large-format LIBs to understand the spatial distribution of active materials, electrode thickness variations, and internal defects in commercial-scale batteries.

In the research [73], XCT was used to investigate the thermal runway of a LIB during a nail penetration test to better understand the safety hazards associated with LIBs; in particular the evolution of internal structural changes, such as electrode deformation and electrolyte decomposition during thermal runaway events. Therefore, gas generation, which is known to indicate an internal short circuit of the cell, and the electrical behavior of the short circuit during the nail penetration test were observed separately.

Other studies emphasized the diverse applications of XCT in investigating various aspects of LIBs, including plating, thermal runaway, and electrode characterization [74]. For example, when gas accumulates inside a battery, swelling or deformation of the casing can occur. XCT can be helpful in detecting excessive gas accumulation or swelling caused by poor packaging or sealing, chemical reactions, and poor electrolyte infiltration [75,76].

Table 3. Studies on predicting the state of LIB based on XCT.

Refs.	Parameter	Error (%)	Battery Type	Instruments	Characteristics
[69]	Defects, inhomogeneity (cathode and anode).	<1	Cylindrical (18650) and pouch	Micro-CT scanner at BAM Microfocus X-ray tube (X-ray WorX GmbH) Flat panel detector (PerkinElmer)	Lithium iron phosphate (LPF) and Lithium cobalt oxide (LCO). Operando experiment. Relationship between beam energy and sample-detector distance. Smaller cells are preferred, the loss of detail is due to the absorption of the thick metal casing.
[70]	Capacity detection (Charge)	<1	pouch	Electrochemical Subsystem (HT-V5C100D100-16) Tomographic-(Phoenix NDT analyzer, GE, Inspection Technologies)	Electrochemical and tomographic measurement. Capacity of LB is a function of the structural parameters of active materials and working condition. Loss of strong active materials of a LB (negative cross-section)
[72]	Degradation, heating and gas generation	<1	Pouch	slip ring (P4 + Compact Slip Ring). FLIR SC5000MB PCO Dimax CMOS camera. Xradia Versa 520 X-ray CT system (Zeiss Xradia Ultra 810) Software-FEI- Avizo Fire 9	LiCoO ₂ positive electrode. Combine high-speed X-ray CT with thermal and electrochemical measurements. Particle microstructures influence the extent and rate of exothermic degradation reactions during thermal runaway.
[74]	Defects and Structural deformation	1	Cylindrical (18650) and pouch	X-ray tube X-ray detector Rotation stage	Anode and cathode: LiCoO ₂ , LiMn ₂ O ₄ , LiNiMnCoO ₂ . Detecting manufacturing-induced defects and structural deformations.
[77]	Material parameter analysis	1.747	Prismatic LPF	Vacuum glove box -ZKX X-ray CT-Phoenix NDT analyzer, GE Inspection. DXR flat type Phoenix datos x 3D and VGStudio max 3.1 software.	Sine function model to identify the 2D tomographic images of electrodes. New insight of battery design and optimization.

Table 3. Cont.

Refs.	Parameter	Error (%)	Battery Type	Instruments	Characteristics
[78]	Inhomogeneity	<1	Coin LIR2032	Neware CT-3008-5 V 10Ma Nano-XCT (UltraXRM-L200, Xradia Inc.)	Cathode: LiFePO ₄ , electrolyte: LiPF ₆ . Multiscale model. Microstructure is reconstructed. Inhomogeneity causes wider distribution. Model is applicable to any LB.
[79]	Optimization of electrode design	1	Cylindrical	Zeiss Xradia Ultra 810 X-ray microscope Software: Carl Zeiss, Avizo and Thermo Fisher Scientific.	Microstructure-resolved 3D model. Guide manufacturing of electrode. Reveal the porosity and tortuosity changes
[80]	Structural changes	1	Cylindrical (18650)	GE Sensing VG Studio MAX	Identification of three main deformation mechanisms: lithiation, thickening, volumetric expansion
[81]	Structural changes	1	Pouch	LiPF ₆ and Li-Tec (HEA40) ZEISS Xradia 520 Versa 3D ZEISS Xradia 810 Ultra 3D Sotware: ZEN 2.5 blue Editions, Carl Zeiss GmbH	Cathode particle cracking. Aluminum current collector corrosion. Cathode swelling.
[82]	Defects, SOH	<1	Cylindrical 18650	Werth TomoScope XS Software: IR ACTIS 5	Work with retired batteries. Computational image recognition algorithm. Structural Similarity Index Measure (SSIM) algorithm.
[83]	Defects	<1	Cylindrical 18650	Basitec XCTS system Climate chambers(Vötsch). NTC sensors GE Phoenix v tome x Volume GraphicsVGStudio MAX 2.0.	Capacity loss was investigated by postmortem. Jelly roll deformation conducted in operando temperature measurements.
[84]	Defects	2	Pouch LiPo	EIS-Autolab potentiostat/galvanostat (PGSTAT100) FRA module (1MHz-0.01MHz) Phoenix V tome X system Perkin Elmer DDD	Postmortem analysis of a failed LB EIS measurements for performance degradation and Xray μ CT for postmortem analysis.

In summary, XCT is the most powerful imaging technique to gain detailed internal information about LIBs. At an industrial level, due to the size and level of precision required, it is one of the most expensive NDT methods, but there are options (desktop-sized) on the market that can be used for research and development. The three-dimensional reconstruction of a battery allows different aspects of the battery to be evaluated such as the distribution of the internal components, the integrity of the electrical connections, the presence of defects, or the uniformity of the structure. Anomalies or defects in the battery become visible in the generated images. This technique can examine any type of battery and has been used to determine structural changes, defects, and even to optimize the design of the electrodes leveraging XCT data. It must be noted that strict safety rules must be observed when performing an XCT test and this needs to be carried out by specialized and trained personnel only, a fact that can limit the exploitation of such a method in some cases.

5. Ultrasonic Testing (UT)

In recent years, UT has also been applied to the field of LIBs evaluation. The use of ultrasound in LIBs is mainly focused on detecting defects and on the real-time monitoring the state of the battery, i.e., its SOC and SOH [85,86]. It is based on the emission and reception of acoustic waves at a frequency range above the audible one, which propagates through the battery material and is reflected back from at the interfaces between components such as electrodes and electrolytes.

The pulse-echo and through-transmission methods are two commonly used ultrasound methods for LIBs. In pulse-echo, a single ultrasonic transducer is placed on the surface of the battery and the ultrasonic waves are transmitted through its inner volume, see Figure 5a. The waves are then reflected back to the transducer when hitting any discontinuities, i.e., any considerable change in the density and speed of sound occurring at the

interfaces between different layers of the battery. By analyzing the reflected waves, it is possible to detect and locate defects in the electrodes, in the separator, and in other internal components. The method is also useful for detecting defects in the packaging such as leaks or cracks. The through-transmission method makes use of two transducers, one on each side of the battery. A transducer is employed to send ultrasonic waves through the battery, while the other one acts as the receiver, see Figure 5b. By analyzing the transmitted waves, it is possible to detect defects in the battery. It can detect shallower defects compared with the pulse-echo, such as shallow microcracks and voids.

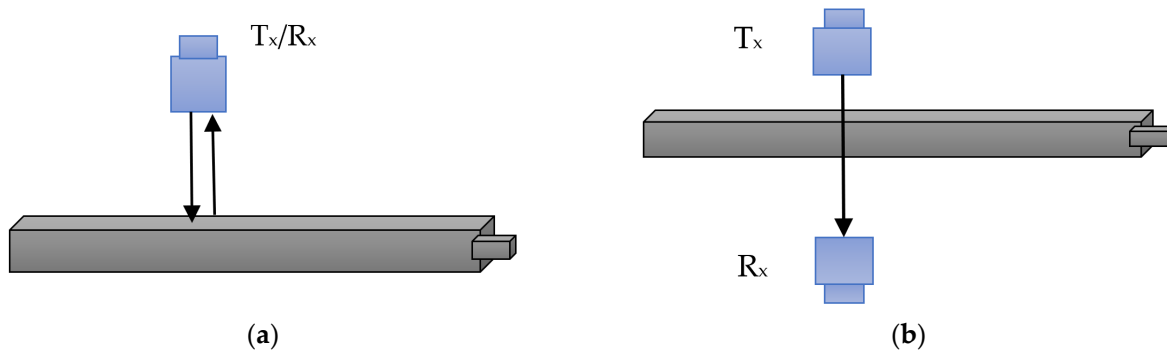


Figure 5. Ultrasonic testing (a) pulse-echo; (b) through-transmission. T_x and R_x stand for transmitter and receiver transducer, respectively.

Although more complex expressions exist depending on the model of wave propagation and the type of elastic constant employed, Equation (5) expresses the ultrasonic longitudinal wave velocity for a homogeneous elastic material, given its Young's modulus (E) and Poisson's ratio (σ) [87].

$$V_p = \sqrt{\frac{C_{ij}}{\rho}} \quad (5)$$

where:

ρ is the material density;

C_{ij} is the material elastic constant.

The acoustic time-of-flight (ToF) and the signal amplitude are two parameters used in ultrasonic testing of LIBs [87]. The ToF measures how long it takes for an ultrasonic signal in pulse-echo mode to return to the receiver. A change in the ultrasonic velocity and/or thickness is thus represented by the ToF. On the other hand, the input acoustic energy, gain, transducer positioning, and contact pressure between the transducer and the LIB are only a few of the variables that may affect signal amplitude, and this should all be taken into account when using it as a proxy. Furthermore, a physical shift in the location of a fault, discontinuity, or interface towards or away from the transducer owing to material expansion or contraction could cause an amplitude peak variation over a specific ToF range, a signal delay, or an extended ToF value [87].

A change in the physical characteristics of the materials at the interface that causes an increase/decrease in the acoustic impedance mismatch at the interface could be the reason for a change in the peak amplitude. For a given material with a fixed V_p the distance L between the emitter and the receiver increases with increasing ToF values, see Equation (6) [88,89], with ρ being the material density.

$$\text{ToF} = \frac{L}{V_p} = \frac{L}{\sqrt{\frac{E}{\rho}}} \quad (6)$$

In addition, powerful ultrasounds can be used to trigger various acoustic emission (AE) events during the charge and discharge cycles. The elastic waves are found to be

related to the battery's condition and are detected by the AE transducer [84,85]. This makes it possible to record more data across a wider frequency range than that of the impinging ultrasonic wave for a more efficient SOH estimation. According to the findings, the root mean square (RMS) of the AE signal can serve as a proxy for SOH, and the frequency range between 270 and 300 kHz can be used to estimate it accurately during discharging [90].

Related Works

Research in work [91] reported an estimation method of SOC and SOH based on ultrasonic guided wave (UGW) technology. In the experiment, a laser Doppler vibrometer and a single fixed piezoelectric transducer are employed. The direct wave signals are subject to a comprehensive analysis using various techniques such as time-domain, frequency-domain, and time-frequency distribution. In addition, the authors found that the sensitivity of UGW technology for estimating the SOC/SOH gradually decreases with battery aging.

In [92–95], a series of approaches to monitor the SOC via ultrasonic ToF measurement are reported. The studies corroborated the link between SOC and ToF and found that the latter is significantly influenced by changes in temperature. Temperature variations and their influence on the ToF measurements have largely been investigated here by a combination of experiments, modelling, in situ monitoring, and sensitivity analyses. This provides a more comprehensive understanding of how SOC, temperature, and ToF are interrelated in LIBs, offering valuable insights for battery management systems and applications in which temperature plays a critical role, such as in electric vehicles and in renewable energy storage.

Furthermore, the air-coupled ultrasound technique has been used to detect defects in a variety of materials, including LIBs [96–99]. This technique uses waves that are transmitted through the air, i.e., are contactless, to detect changes in the material's structure. In LIBs, air-coupled ultrasound shows good potential to detect defects such as delamination, cracking, and voids in the electrodes and separators, as well as for estimating SOC. By detecting these defects early, air-coupled ultrasound can help prevent catastrophic battery failure and improve the overall safety and performance of LIBs [100,101].

In other studies [102,103], MLTs, have also been used to link acoustic signatures and the SOC. The processing of entire waveforms is shown, without any prior feature selection, creating streamlined workflows of a regression model for training and evaluation [104].

Finally, in [58], a new method for the joint estimation of LIBs' SOC and temperature is proposed by leveraging ultrasonic reflected waves. The main benefit of such a method is the ability to analyze the internal structure of the battery as long as its state changes, by selecting multiple feature indicators, and analyzing the effective intervals of ultrasonic signals. Additionally, the proposed method uses a virtual sample generation algorithm for data augmentation, which can improve the accuracy of the estimation. In addition, combining UT with IR data for detecting potential gas production is a powerful and comprehensive approach for battery health assessment. In fact, UT enables inspection of the internal structure of a battery, identifying potential defects that might compromise its integrity. Simultaneously, the IR method allows the temperature variations on the battery's surface to be monitored, highlighting areas with abnormal thermal signatures, which can indicate gas buildup or other internal issues. By integrating these two techniques, a holistic understanding of the battery's condition is gained, enabling early detection of problems related to gas production, thermal imbalances, or structural abnormalities. This approach is pivotal for ensuring the safety and reliability of LIBs in various applications, from electric vehicles to renewable energy storage systems.

Table 4 presents a set of scientific articles describing the studies performed using UT.

Table 4. Studies on predicting SOC of LB based on Ultrasound.

Refs.	Parameter	Error (%)	Battery Type	Experimental Setup	Characteristics
[93]	SOC	1.29–16.85	Pouch	Piezo disc type: AB1290B-LW100-R Microcontroller Transmitter circuit Receiver circuit. K-type thermocouple	Correlation between SOC and TOF. It can be directly implemented into a BMS. Two surface-mounted sensors.
[105]	SOC	~1	Pouch	LiNi _{0.6} -Mn _{0.2} Co _{0.2} O ₂ Four types of transducers: longitudinal (Olympus V103 and C106) and shear (Olympus V153 and V154).	Monitoring charge/discharge LBs. Longitudinal wave velocity is linearly related to SOC. Temperature effect is related to SOC. Signal processing algorithms for amplitude, wave velocity, and attenuation.
[95]	SOC	~1	Pouch	Phascan PA32/64 UT 2:4 NEWARE-CT-4008T-5V12A ST8450 Visual Thermal Imager	Amplitude is correlated with volume changes. It is affected by the physical properties of battery layers, charge-discharge parameters, and temperature.
[101]	SOC	<2	Pouch	CEA-LM36 (NiMnCoO ₂) Air-coupled Ultrasonic system-NAUT-21 Pulser/receiver (JPR600C) NI-PXI-5114 signal acquisition card.	Real-time measurement SOC. Fast amplitude has an approximately linear relationship with SOC. Air-coupled ultrasound is extremely sensitive to the gas bubbles.
[106]	layer properties and SOC	~1	Pouch	Harisonic I3-0504-S; V109-RM, V121-RM, Olympus	Inner structure of LIBs: number of layers, average thicknesses of electrodes, image of internal layers, and SOC. Pulse-echo configuration.
[94]	SOC-SOH	~1	Pouch	Pouch cells (LiCoO ₂ , LiFePO ₄) Neware BTS-3000 cycler Epoch 600 ultrasonic pulser-receiver. Olympus-2.25 MHz transducers. SONO 600 ultrasonic gel.	Ultrasonic measurements (SOC) and machine learning model (SOH). Electrochemical-mechanical relationships using higher frequency ultrasonic.
[107]	SOC	3.5	Pouch	Piezokeramisches EPZ-Serie-6400 Hz MASMesssystem Software: CANWARE08_ISC	SoC can be determined without a reference electrode. Method does not rely on electric measurements. It offers due to rapid measurement sequential screening of batteries within battery packs.
[108]	SOC	~1	Pouch	RIGOL: DG1022Z Aigtek: ATA-2021H Piezoelectric transducer 125 kHz LDV SOPOP: LV-S01	State characterization of LB based on (UGW) scanning is carried out. Characteristic parameters extracted from a single point. Line scanning multi-point UGW signals are listed.
[109]	SOC	~3	Pouch, Cylindrical and Alkaline AA	EPOCH-600 Neware BTS-3000 cycler Ultrasonic pulser-receiver 2.25 MHz transducers.	Non-invasive, in operando method. 1D acoustic conservational law model. Two transducers: one in pulse-echo (reflection) mode and the other in transmission mode. The model does not include many of the non-linear physical processes.
[110]	SOC, SOH	<1	Pouch	Piezoelectric disc transducers ZT-5A Hysol E20HP NEWARE BST-9000	Experimental and analytical studies. Acoustic-ultrasonic guided waves SoC/SOH can be accurately predicted using guided wave data on demand.
[111]	SOH, electrode or RUL	~1	Pouch	Commercial-2800mAh battery. Epoch 650 ultrasonic Piezoelectric transducer 5 MHz-M110-RM. Nikon XT-225; Nikon CT Agent-visualization Avizo Fire	Real-time data, diagnostic tool. Measurements on a commercial mobile phone battery. X-ray CT to ascertain the internal architecture and features.
[112]	SOH	0.02	Pouch	Data acquisition card Power amplifier Oscilloscope Machine Learning(Classification and Regression Trees)	Machine prediction model for batteries. Complex data-driven model- SOH, big-data, AI, IoT.
[101]	SOC	~1–2	Pouch	Ultrasonic pulser/receiver (JPR600C), NI-PXI-5114-signal acquisition card Air-coupled dedicated transducer.	Air-coupled ultrasound. Biot's fluid-saturated porous media model. Real-time monitoring.
[113]	degradation effects	~1	Pouch	(Kokam SLPB526495) EIS, Train gauge, strip (Hottinger Baldwin Messtechnik 6/120A LY11) Ultrasound measurement system (Safion US100, prototype) Adiabatic HEL BTC500 calorimeter K type thermocouples	In operando measurement techniques (fast impedance spectroscopy and ultrasonic waves)-in real time.

To sum up, the use of ultrasound has spread over the years in the industrial sector, and the automotive industry is not an exception. In recent years, several studies have been carried out on the use of UT for the detection of failures in the batteries of electric vehicles. Most studies suggest that combining ultrasounds with machine learning techniques can provide a more reliable estimate of SOH and SOC [114]. The accuracy of the measurements can vary between 1 and 5% depending on the environmental conditions, transducers or transmission method employed.

6. Discussion

The accurate estimation of various parameters, such as charge/discharge characteristics, structural changes, heat generation, etc., are crucial for ensuring the safe and controlled usage of LIBs across diverse applications. In this framework, NDT methods have proven to be invaluable tools for assessing LIBs in both research and industrial contexts. Their versatility, sensitivity, cost-effectiveness, in operando evaluation capabilities, and accuracy enable the acquisition of detailed information about battery condition and performance, without causing any damage. These methods contribute significantly to enhancing battery safety, reliability, efficiency, and real-time monitoring, all of which are vital for advancing energy storage technologies. Thus, the main goal of this review paper is to serve as a foundational resource for professionals seeking to apply these techniques in real-world applications by conducting an accurate literature review based on the estimation parameters and instruments used in four NDT different techniques, i.e., electromechanical impedance spectroscopy (EIS), infrared thermography (IRT), X-ray computer tomography (XCT), and ultrasonic testing (UT). Note that this set of techniques has been chosen as they are widely adopted in both research and industrial battery-related applications.

As demonstrated, choosing the most suitable NDT method for evaluating LIBs is a complex and pivotal decision in both research and industrial applications. The choice of an appropriate method depends on the specific application and the characteristics of the LIB under analysis, including material type, defect size, and desired level of accuracy. The following characteristics have been analyzed in this review:

- *Versatility and Effectiveness:* the explored NDT methods provide researchers and engineers with a wide range of tools to evaluate LIBs, each offering unique advantages in terms of the information they can provide.
- *Cost:* it is essential to note that the implementation of an NDT can involve a significant initial investment in equipment and training. Methods such as XCT and IR have relatively high initial costs.
- *In Operando Evaluation:* the capability to evaluate batteries during their operation is a crucial advantage of NDT technologies. This allows real-time measurements and monitoring of battery performance to be used under real-world conditions.
- *Measurement Accuracy:* some methods provide more accurate measurements in specific aspects, such as leak detection or structural integrity assessment, while others may be better suited for assessing the state of charge or overall battery health. This aspect has been discussed in detail in the manuscript.

A visual comparison of the abovementioned set of characteristics is depicted in Figure 6. As a general guideline, EIS is considered the most suitable method for its balance between accuracy and equipment costs, and it can provide a range of meaningful parameters depending on the selection of the underlying physical model:

Although sensitive to external factors like environmental temperature or non-uniform heating, IRT is preferred when thermal anomalies should be detected. For inferring the presence of internal structural changes or defects, XCT represents the optimal choice, albeit requiring expensive equipment and specialized personnel. It is primarily used in R&D applications rather than in industrial production for in-line monitoring. UT methods represent a versatile alternative, although the accuracy of results may be limited by environmental factors such as temperature and humidity, and the need for couplants.

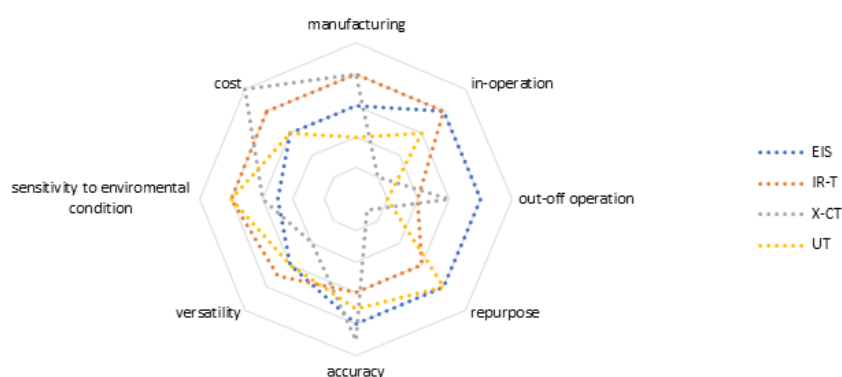


Figure 6. Comparative analysis of the selected NDT methods.

7. Conclusions and Future Directions

This work provides a review of recent contributions related to NDT for evaluating LIBs. Today's NDT methods can detect signs of deformation, leaks, swelling, corrosion, and other visible and non-visible signs of deterioration. These methods can also inspect battery connections, terminals, and internal material damage for potential manufacturing issues. The specific selection of an NDT method may depend on the type of defects to be identified and the production or monitoring environment in which the inspection takes place.

Choosing the appropriate method depends on the application and the type of information required from the battery, such as state of charge (SOC), internal or external defects, state of health (SOH), accessibility, heat generation, and real-time measurements. Future developments in NDT methods, both within the field and in other industrial contexts, may mutually drive advancements in LIBs monitoring.

In a broader context, the future of NDT is undoubtedly going to be shaped by technological advancements, the integration of AI, and a focus on improving the accuracy and efficiency of existing methods. Researchers can contribute to this field by working on AI algorithms, sensor technology, advanced imaging techniques, quantitative NDT, and sustainability initiatives as well.

Another promising advancement is the adoption of advanced data analysis. With the increasing use of sensors and data collection tools, substantial data are generated during NDT inspections. Extracting valuable insights from large data for making more informed decisions about the materials and structures to be tested is a pivotal future direction.

As a conclusion, environmental impact and sustainability are playing an increasingly important role in the choice and further development of NDT processes. Strong research efforts are advisable in exploring ways to reduce waste, energy consumption, and the environmental footprint of NDT processes.

Author Contributions: Conceptualization, X.C.A.C. and G.C.; methodology, X.C.A.C., S.L. and G.C.; validation, X.C.A.C., S.L., M.R. and G.C.; formal analysis, X.C.A.C., S.L., M.R. and G.C.; investigation, X.C.A.C., S.L. and G.C.; data curation, X.C.A.C. and S.L.; writing—original draft preparation, X.C.A.C.; writing—review and editing, X.C.A.C., S.L., M.R. and G.C.; supervision, M.R. and G.C.; project administration, X.C.A.C. and G.C.; funding acquisition, G.C. All authors have read and agreed to the published version of the manuscript.

Funding: This work was funded by the Next Generation EU–Italian NRRP, Mission 4, Component 2, Investment 1.5, call for the creation and strengthening of ‘Innovation Ecosystems’, building ‘Territorial R&D Leaders’ (Directorial Decree n. 2021/3277)—project Tech4You—Technologies for climate change adaptation and quality of life improvement, n. ECS0000009. This work reflects only the authors' views and opinions, neither the Ministry for University and for Research nor the European Commission can be considered responsible for them.

Data Availability Statement: The data presented in this study are available on request from the corresponding author.

Conflicts of Interest: The authors declare no conflict of interest.

References

- Zhang, H.; Sun, C.; Ge, M. Review of the Research Status of Cost-Effective Zinc–Iron Redox Flow Batteries. *Batteries* **2022**, *8*, 202. [[CrossRef](#)]
- Elibama. *European Li-Ion Battery Advanced Manufacturing for Electric Vehicles Non-Destructive-Testing*; University of Newcastle: Newcastle upon Tyne, UK, 2014; p. 14.
- Tomaszewska, A.; Chu, Z.; Feng, X.; O’Kane, S.; Liu, X.; Chen, J.; Ji, C.; Endler, E.; Li, R.; Liu, L.; et al. Lithium-ion battery fast charging: A review. *eTransportation* **2019**, *1*, 100011. [[CrossRef](#)]
- Rangarajan, S.S.; Sunddararaj, S.P.; Sudhakar, A.V.V.; Shiva, C.K.; Subramaniam, U.; Collins, E.R.; Senju, T. Lithium-Ion Batteries—The Crux of Electric Vehicles with Opportunities and Challenges. *Clean Technol.* **2022**, *4*, 908–930. [[CrossRef](#)]
- Bai, Y.; Muralidharan, N.; Sun, Y.-K.; Passerini, S.; Stanley Whittingham, M.; Belharouak, I. Energy and environmental aspects in recycling lithium-ion batteries: Concept of Battery Identity Global Passport. *Mater. Today* **2020**, *41*, 304–315. [[CrossRef](#)]
- Liang, Y.; Zhao, C.Z.; Yuan, H.; Chen, Y.; Zhang, W.; Huang, J.Q.; Yu, D.; Liu, Y.; Titirici, M.M.; Chueh, Y.L.; et al. A review of rechargeable batteries for portable electronic devices. *InfoMat* **2019**, *1*, 6–32. [[CrossRef](#)]
- Etiemble, A.; Besnard, N.; Adrien, J.; Tran-Van, P.; Gautier, L.; Lestriez, B.; Maire, E. Quality control tool of electrode coating for lithium-ion batteries based on X-ray radiography. *J. Power Sources* **2015**, *298*, 285–291. [[CrossRef](#)]
- Wang, Q.; Ping, P.; Zhao, X.; Chu, G.; Sun, J.; Chen, C. Thermal runaway caused fire and explosion of lithium ion battery. *J. Power Sources* **2012**, *208*, 210–224. [[CrossRef](#)]
- Feng, X.; Pan, Y.; He, X.; Wang, L.; Ouyang, M. Detecting the internal short circuit in large-format lithium-ion battery using model-based fault-diagnosis algorithm. *J. Energy Storage* **2018**, *18*, 26–39. [[CrossRef](#)]
- Olabi, A.G.; Maghrabie, H.M.; Adhari, O.H.K.; Sayed, E.T.; Yousef, B.A.A.; Salameh, T.; Kamil, M.; Abdelkareem, M.A. Battery thermal management systems: Recent progress and challenges. *Int. J. Thermofluids* **2022**, *15*, 100171. [[CrossRef](#)]
- Barbosa, J.C.; Gonçalves, R.; Costa, C.M.; Lanceros-Mendez, S. Recent Advances on Materials for Lithium-Ion Batteries. *Energies* **2021**, *14*, 3145. [[CrossRef](#)]
- Lamb, J.; Orendorff, C.J. Evaluation of mechanical abuse techniques in lithium ion batteries. *J. Power Sources* **2014**, *247*, 189–196. [[CrossRef](#)]
- Wang, H.; Lara-Curzio, E.; Rule, E.T.; Winchester, C.S. Mechanical abuse simulation and thermal runaway risks of large-format Li-ion batteries. *J. Power Sources* **2017**, *342*, 913–920. [[CrossRef](#)]
- Duan, J.; Tang, X.; Dai, H.; Yang, Y.; Wu, W.; Wei, X.; Huang, Y. Building Safe Lithium-Ion Batteries for Electric Vehicles: A Review. *Electrochem. Energy Rev.* **2020**, *3*, 1–42. [[CrossRef](#)]
- Lambert, S.M.; Armstrong, M.; Attidekou, P.S.; Christensen, P.A.; Widmer, J.D.; Wang, C.; Scott, K. Rapid nondestructive-testing technique for in-line quality control of li-ion batteries. *IEEE Trans. Ind. Electron.* **2017**, *64*, 4017–4026. [[CrossRef](#)]
- Büyüköztürk, O.; Taşdemir, M.A. *Nondestructive Testing of Materials and Structures*; Springer: Dordrecht, The Netherlands, 2013; Volume 6.
- Aryan, P.; Sampath, S.; Sohn, H. An overview of non-destructive testing methods for integrated circuit packaging inspection. *Sensors* **2018**, *18*, 1981. [[CrossRef](#)] [[PubMed](#)]
- Li, Y.; Guo, J.; Pedersen, K.; Gurevich, L.; Stroe, D.-I. Recent Health Diagnosis Methods for Lithium-Ion Batteries. *Batteries* **2022**, *8*, 72. [[CrossRef](#)]
- McGovern, M.E.; Bruder, D.D.; Huemiller, E.D.; Rinker, T.J.; Bracey, J.T.; Sekol, R.C.; Abell, J.A. A review of research needs in nondestructive evaluation for quality verification in electric vehicle lithium-ion battery cell manufacturing. *J. Power Sources* **2023**, *561*, 232742. [[CrossRef](#)]
- Xu, J.; Sun, C.; Ni, Y.; Lyu, C.; Wu, C.; Zhang, H.; Yang, Q.; Feng, F. Fast Identification of Micro-Health Parameters for Retired Batteries Based on a Simplified P2D Model by Using Padé Approximation. *Batteries* **2023**, *9*, 64. [[CrossRef](#)]
- Meddings, N.; Heinrich, M.; Overney, F.; Lee, J.-S.; Ruiz, V.; Napolitano, E.; Seitz, S.; Hinds, G.; Raccichini, R.; Gaberscek, M. Application of electrochemical impedance spectroscopy to commercial Li-ion cells: A review. *J. Power Sources* **2020**, *480*, 228742. [[CrossRef](#)]
- Padha, B.; Verma, S.; Mahajan, P.; Arya, S. Electrochemical Impedance Spectroscopy (EIS) Performance Analysis and Challenges in Fuel Cell Applications. *J. Electrochem. Sci. Technol.* **2022**, *13*, 167–176. [[CrossRef](#)]
- Lazanas, A.C.; Prodromidis, M.I. Electrochemical Impedance Spectroscopy—A Tutorial. *ACS Meas. Sci. Au* **2023**, *3*, 162–193. [[CrossRef](#)] [[PubMed](#)]
- Hogg, B.-I.; Waldmann, T.; Wohlfahrt-Mehrens, M. 4-Electrode Full Cells for Operando Li⁺ Activity Measurements and Prevention of Li Deposition in Li-Ion Cells. *J. Electrochem. Soc.* **2020**, *167*, 090525. [[CrossRef](#)]
- Carthy, K.; Gullapalli, H.; Kennedy, T. Real-time internal temperature estimation of commercial Li-ion batteries using online impedance measurements. *J. Power Sources* **2022**, *519*, 230786.
- Zheng, Y.; Shi, Z.; Guo, D.; Dai, H.; Han, X. A simplification of the time-domain equivalent circuit model for lithium-ion batteries based on low-frequency electrochemical impedance spectra. *J. Power Sources* **2021**, *489*, 229505. [[CrossRef](#)]
- Fernández Pulido, Y.; Blanco, C.; Anseán, D.; García, V.M.; Ferrero, F.; Valledor, M. Determination of suitable parameters for battery analysis by Electrochemical Impedance Spectroscopy. *Measurement* **2017**, *106*, 1–11. [[CrossRef](#)]

28. Choi, W.; Shin, H.C.; Kim, J.M.; Choi, J.Y.; Yoon, W.S. Modeling and applications of electrochemical impedance spectroscopy (Eis) for lithium-ion batteries. *J. Electrochem. Sci. Technol.* **2020**, *11*, 1–13. [CrossRef]
29. Andre, D.; Meiler, M.; Steiner, K.; Walz, H.; Soczka-Guth, T.; Sauer, D.U. Characterization of high-power lithium-ion batteries by electrochemical impedance spectroscopy. II: Modelling. *J. Power Sources* **2011**, *196*, 5349–5356. [CrossRef]
30. Habte, B.T.; Jiang, F. Effect of microstructure morphology on Li-ion battery graphite anode performance: Electrochemical impedance spectroscopy modeling and analysis. *Solid State Ionics* **2018**, *314*, 81–91. [CrossRef]
31. Westerhoff, U.; Kurbach, K.; Lienesch, F.; Kurrat, M. Analysis of Lithium-Ion Battery Models Based on Electrochemical Impedance Spectroscopy. *Energy Technol.* **2016**, *4*, 1620–1630. [CrossRef]
32. Li, D.; Wang, L.; Duan, C.; Li, Q.; Wang, K. Temperature prediction of lithium-ion batteries based on electrochemical impedance spectrum: A review. *Int. J. Energy Res.* **2022**, *46*, 10372–10388. [CrossRef]
33. Lyu, C.; Zhang, T.; Luo, W.; Wei, G.; Ma, B.; Wang, L. SOH Estimation of Lithium-ion Batteries Based on Fast Time Domain Impedance Spectroscopy. In Proceedings of the 2019 14th IEEE Conference on Industrial Electronics and Applications (ICIEA), Xi'an, China, 19–21 June 2019; pp. 2142–2147.
34. Eddahech, A.; Briat, O.; Bertrand, N.; Delétage, J.-Y.; Vinassa, J.-M. Behavior and state-of-health monitoring of Li-ion batteries using impedance spectroscopy and recurrent neural networks. *Int. J. Electr. Power Energy Syst.* **2012**, *42*, 487–494. [CrossRef]
35. Li, D.; Yang, D.; Li, L.; Wang, L.; Wang, K. Electrochemical Impedance Spectroscopy Based on the State of Health Estimation for Lithium-Ion Batteries. *Energies* **2022**, *15*, 6665. [CrossRef]
36. Zhang, Y.; Tang, Q.; Zhang, Y.; Wang, J.; Stimming, U.; Lee, A.A. Identifying degradation patterns of lithium ion batteries from impedance spectroscopy using machine learning. *Nat. Commun.* **2020**, *11*, 1706. [CrossRef] [PubMed]
37. Galeotti, M.; Ciná, L.; Giannamico, C.; Cordiner, S. Performance analysis and SOH (state of health) evaluation of lithium polymer batteries through electrochemic. *Energy* **2015**, *89*, 678–686. [CrossRef]
38. Ezpeleta, I.; Freire, L.; Mateo-Mateo, C.; Nóvoa, X.R.; Pintos, A.; Valverde-Pérez, S. Characterisation of Commercial Li-Ion Batteries Using Electrochemical Impedance Spectroscopy. *ChemistrySelect* **2022**, *7*, e202104464. [CrossRef]
39. Zhang, Q.; Huang, C.G.; Li, H.; Feng, G.; Peng, W. Electrochemical Impedance Spectroscopy Based State-of-Health Estimation for Lithium-Ion Battery Considering Temperature and State-of-Charge Effect. *IEEE Trans. Transp. Electrif.* **2022**, *8*, 4633–4645. [CrossRef]
40. Chang, C.; Wang, S.; Jiang, J.; Gao, Y.; Jiang, Y.; Liao, L. Lithium-Ion Battery State of Health Estimation Based on Electrochemical Impedance Spectroscopy and Cuckoo Search Algorithm Optimized Elman Neural Network. *J. Electrochem. Energy Convers. Storage* **2022**, *19*, 030912. [CrossRef]
41. Alfredo Osornio-Rios, R.; Antonino-Daviu, J.A.; De Jesus Romero-Troncoso, R. Recent industrial applications of infrared thermography: A review. *IEEE Trans. Ind. Inf.* **2019**, *15*, 615–625. [CrossRef]
42. Hou, F.; Zhang, Y.; Zhou, Y.; Zhang, M.; Lv, B.; Wu, J. Review on Infrared Imaging Technology. *Sustainability* **2022**, *14*, 11161. [CrossRef]
43. Balakrishnan, G.K.; Yaw, C.T.; Koh, S.P.; Abedin, T.; Raj, A.A.; Tiong, S.K.; Chen, C.P. A Review of Infrared Thermography for Condition-Based Monitoring in Electrical Energy: Applications and Recommendations. *Energies* **2022**, *15*, 6000. [CrossRef]
44. Usamentiaga, R.; Venegas, P.; Guerediaga, J.; Vega, L.; Molleda, J.; Bulnes, F. Infrared Thermography for Temperature Measurement and Non-Destructive Testing. *Sensors* **2014**, *14*, 12305–12348. [CrossRef] [PubMed]
45. Pesaran, A.A.; Burch, S.D. *Thermal Performance of EV and HEV Battery Modules and Packs Prepared under FWP HV71*; National Renewable Energy Laboratory: Golden, CO, USA, 1997; p. 997.
46. Giannicchele, L.; D'Alessandro, V.; Falone, M.; Ricci, R. Thermal behaviour assessment and electrical characterisation of a cylindrical Lithium-ion battery using infrared thermography. *Appl. Thermal Eng.* **2022**, *205*, 117974. [CrossRef]
47. Wang, Z.-j.; Li, Z.-q.; Liu, Q. Infrared thermography non-destructive evaluation of lithium-ion battery. In *International Symposium on Photoelectronic Detection and Imaging 2011: Advances in Infrared Imaging and Applications*; SPIE: Beijing, China, 2011; pp. 1237–1244.
48. Bazinsky, S.J.; Wang, X. Predicting heat generation in a lithium-ion pouch cell through thermography and the lumped capacitance model. *J. Power Sories* **2016**, *305*, 97–105. [CrossRef]
49. Rani, M.F.H.; Razlan, Z.M.; Shahriman, A.B.; Ibrahim, Z.; Wan, W.K. Comparative study of surface temperature of lithium-ion polymer cells at different discharging rates by infrared thermography and thermocouple. *Int. J. Heat Mass Transf.* **2020**, *153*, 119595. [CrossRef]
50. Goutam, S.; Timmermans, J.M.; Omar, N.; Van den Bossche, P.; Van Mierlo, J. Comparative study of surface temperature behavior of commercial li-ion pouch cells of different chemistries and capacities by infrared thermography. *Energies* **2015**, *8*, 8175–8192. [CrossRef]
51. Liu, Y.; Xu, S.; Wang, Y.; Dong, H. Non-contact Steady-State Thermal Characterization of Lithium-Ion Battery Plates Using Infrared Thermography. *Int. J. Thermophys.* **2022**, *43*, 131. [CrossRef]
52. Mohanty, D.; Hockaday, E.; Hensley, D.K.; Daniel, C.; Wood, I.D. Effect of electrode manufacturing defects on electrochemical performance of lithium-ion batteries. *J. Power Sources* **2016**, *312*, 70–79. [CrossRef]
53. Mohanty, D.; Li, J.; Born, R.; Maxey, L.C.; Dinwiddie, R.B.; Daniel, C.; Wood, D.L. Non-destructive evaluation of slot-die-coated lithium secondary battery electrodes by in-line laser caliper and IR thermography methods. *Anal. Methods* **2014**, *6*, 674–683. [CrossRef]

54. Robinson, J.B.; Engebretsen, E.; Finegan, D.P.; Darr, J.; Hinds, G.; Shearing, P.R.; Brett, D.J.L. Detection of internal defects in lithium-ion batteries using lock-in thermography. *ECS Electrochem. Lett.* **2015**, *4*, A106–A109. [[CrossRef](#)]
55. Stoynova, A.; Bonev, B.; Rizanov, S. Thermographic Study of Thermal Processes during Battery Charging and Discharging. In Proceedings of the 2021 44th International Spring Seminar on Electronics Technology (ISSE), Bautzen, Germany, 5–9 May 2021.
56. Zhang, G.; Tian, H.; Ge, S.; Marple, D.; Sun, F.; Wang, C.-Y. Visualization of self-heating of an all climate battery by infrared thermography. *J. Power Sources* **2018**, *376*, 111–116. [[CrossRef](#)]
57. Zhou, X.; Hsieh, S.-J.; Peng, B.; Hsieh, D. Cycle life estimation of lithium-ion polymer batteries using artificial neural network and support vector. *Microelectron. Reabil.* **2017**, *79*, 48–58. [[CrossRef](#)]
58. Zhang, R.; Li, X.; Sun, C.; Yang, S.; Tian, Y.; Tian, J. State of Charge and Temperature Joint Estimation Based on Ultrasonic Reflection Waves for Lithium-Ion Battery Applications. *Batteries* **2023**, *9*, 335. [[CrossRef](#)]
59. Wang, Y.; Miller, J.D. Current developments and applications of micro-CT for the 3D analysis of multiphase mineral systems in geometallurgy. *Earth-Sci. Rev.* **2020**, *211*, 103406. [[CrossRef](#)]
60. De Chiffre, L.; Carmignato, S.; Kruth, J.P.; Schmitt, R.; Weckenmann, A. Industrial applications of computed tomography. *CIRP Ann.* **2014**, *63*, 655–677. [[CrossRef](#)]
61. Deng, Z.; Lin, X.; Huang, Z.; Meng, J.; Zhong, Y.; Ma, G.; Zhou, Y.; Shen, Y.; Ding, H.; Huang, Y. Recent Progress on Advanced Imaging Techniques for Lithium-Ion Batteries. *Adv. Energy Mater.* **2021**, *11*, 2000806. [[CrossRef](#)]
62. Chen, W.; Chen, X.; Chen, W.; Jiang, Z. In Situ Atomic Force Microscopy and X-ray Computed Tomography Characterization of All-Solid-State Lithium Batteries: Both Local and Overall. *Energy Technol.* **2023**, *11*, 2201372. [[CrossRef](#)]
63. Ciliberti, G.A.; Janello, P.; Jahnke, P.; Keuthage, L. Potentials of Full-Vehicle CT Scans within the Automotive Industry. In Proceedings of the 19th World Conference on Non-Destructive Testing (WCNDT 2016), Munich, Germany, 13–17 June 2016; pp. 13–17.
64. Kentaro, O.; Yugo, K.; Yutaka, H.; Toshiyuki, K. *Analysis Technologies for Quality Improvement in Magnet Wires of Electrified Vehicles Featured Topic*; SUMITOMO ELECTRIC: Osaka, Japan, 2020; pp. 1–5.
65. Le Houux, J.; Kramer, D. X-ray tomography for lithium ion battery electrode characterisation—A review. *Energy Rep.* **2021**, *7*, 9–14. [[CrossRef](#)]
66. Lewis, J.A.; Cortes, F.J.Q.; Liu, Y.; Miers, J.C.; Verma, A.; Vishnugopi, B.S.; Tippens, J.; Prakash, D.; Marchese, T.S.; Han, S.Y.; et al. Linking void and interphase evolution to electrochemistry in solid-state batteries using operando X-ray tomography. *Nat. Mater.* **2021**, *20*, 503–510. [[CrossRef](#)]
67. Liu, J.; Wang, T.; Yu, J.; Li, S.; Ma, H.; Liu, X. Review of the Developments and Difficulties in Inorganic Solid-State Electrolytes. *Materials* **2023**, *16*, 2510. [[CrossRef](#)]
68. Guo, Y.; Wu, S.; He, Y.-B.; Kang, F.; Chen, L.; Li, H.; Yang, Q.-H. Solid-state lithium batteries: Safety and prospects. *eScience* **2022**, *2*, 138–163. [[CrossRef](#)]
69. Dayani, S.; Markotter, H.; Schmidt, A.; Putra Widjaja, M. Multi-level X-ray computed tomography (XCT) investigations of commercial lithium-ion batteries from cell to parti. *J. Energy Storage* **2023**, *66*, 107453. [[CrossRef](#)]
70. Li, L.; Hou, J. Capacity detection of electric vehicle lithium-ion batteries based on X-ray computed tomography. *RSC Adv.* **2018**, *8*, 25325–25333. [[CrossRef](#)] [[PubMed](#)]
71. Ho, A.S.; Parkinson, D.Y.; Finegan, D.P.; Trask, S.E.; Jansen, A.N.; Tong, W.; Balsara, N.P. 3D Detection of Lithiation and Lithium Plating in Graphite Anodes during Fast Charging. *ACS Nano* **2021**, *15*, 10480–10487. [[CrossRef](#)]
72. Finegan, D.P.; Scheel, M.; Robinson, J.B.; Tjaden, B.; Di Michiel, M.; Hinds, G.; Brett, D.J.L.; Shearing, P.R. Investigating lithium-ion battery materials during overcharge-induced thermal runaway: An operando and multi-scale X-ray CT study. *Phys. Chem. Chem. Phys.* **2016**, *18*, 30912–30919. [[CrossRef](#)] [[PubMed](#)]
73. Yokoshima, T.; Mukoyama, D.; Maeda, F.; Osaka, T.; Takazawa, K.; Egusa, S. Operando Analysis of Thermal Runaway in Lithium Ion Battery during Nail-Penetration Test Using an X-ray Inspection System. *J. Electrochem. Soc.* **2019**, *166*, A1243–A1250. [[CrossRef](#)]
74. Wu, Y.; Saxena, S.; Xing, Y.; Wang, Y.; Li, C.; Yung, W.; Pecht, M. Analysis of Manufacturing-Induced Defects and Structural Deformations in Lithium-Ion Batteries Using Computed Tomography. *Energies* **2018**, *11*, 925. [[CrossRef](#)]
75. Chen, C.; Wei, Y.; Zhao, Z.; Zou, Y.; Luo, D. Investigation of the swelling failure of lithium-ion battery packs at low temperatures using 2D/3D X-ray computed tomography. *Electrochim. Acta* **2019**, *305*, 65–71. [[CrossRef](#)]
76. Fahy, K.F.; Shafaque, H.W.; Shrestha, P.; Ouellette, D.; Ge, N.; Ikeda, N.; Kotaka, T.; Tabuchi, Y.; Bazylak, A. Tracking Battery Swelling in Uncompressed Li-Ion Cells via in-Operando X-ray Radiography and Micro-Tomography. *ECS Meet. Abstr.* **2019**, *MA2019-02*, 338. [[CrossRef](#)]
77. Hou, J.; Wang, H.; Qi, L.; Wu, W.; Li, L.; Lai, R.; Feng, X.; Gao, X.; Wu, W.; Cai, W. Material parameter analysis of lithium-ion battery based on laboratory X-ray computed tomography. *J. Power Sources* **2022**, *549*, 232131. [[CrossRef](#)]
78. Kashkooli Ali, G.; Farhad, S.; Dong Un, L.; Kun, F.; Shawn, L.; Komini Babu, S.; Zhu, L.; Chen, Z. Multiscale modeling of lithium-ion battery electrodes based on nano-sca. *J. Power Sources* **2016**, *307*, 496–509. [[CrossRef](#)]
79. Lu, X.; Bertei, A.; Finegan, D.P.; Tan, C.; Daemi, S.R.; Weaving, J.S.; O'Regan, K.B.; Heenan, T.M.M.; Hinds, G.; Kendrick, E.; et al. 3D microstructure design of lithium-ion battery electrodes assisted by X-ray nano-computed tomography and modelling. *Nat. Commun.* **2020**, *11*, 2079. [[CrossRef](#)]

80. Pfrang, A.; Kersys, A.; Kriston, A.; Scurtu, R.-G.; Marinaro, M.; Wohlfahrt-Mehrens, M. Deformation from Formation Until End of Life: Micro X-ray Computed Tomography of Silicon Alloy Containing 18650 Li-Ion Cells. *J. Electrochem. Soc.* **2023**, *170*, 030548. [\[CrossRef\]](#)
81. Rahe, C.; Kelly, S.T.; Rad, M.N.; Sauer, D.U.; Mayer, J.; Figgemeier, E. Nanoscale X-ray imaging of ageing in automotive lithium ion battery cells. *J. Power Sources* **2019**, *433*, 126631. [\[CrossRef\]](#)
82. Ran, A.; Chen, S.; Zhang, S.; Liu, S.; Zhou, Z.; Nie, P.; Qian, K.; Fang, L.; Zhao, S.X.; Li, B.; et al. A gradient screening approach for retired lithium-ion batteries based on X-ray computed tomography images. *RSC Adv.* **2020**, *10*, 19117–19123. [\[CrossRef\]](#)
83. Waldmann, T.; Gorse, S.; Samtleben, T.; Schneider, G.; Knoblauch, V.; Wohlfahrt-Mehrens, M. A Mechanical Aging Mechanism in Lithium-Ion Batteries. *J. Electrochem. Soc.* **2014**, *161*, A1742–A1747. [\[CrossRef\]](#)
84. Yufit, V. Investigation of lithium-ion polymer battery cell failure using X-ray computed tomography. *Electrochem. Commun.* **2011**, *13*, 608–610. [\[CrossRef\]](#)
85. Popp, H.; Koller, M.; Jahn, M.; Bergmann, A. Mechanical methods for state determination of Lithium-Ion secondary batteries: A review. *J. Energy Storage* **2020**, *32*, 101859. [\[CrossRef\]](#)
86. Montoya-Bedoya, S.; Bernal, M.; Sabogal-Moncada, L.A.; Martinez-Tejada, H.V.; Garcia-Tamayo, E. Noninvasive ultrasound for Lithium-ion batteries state estimation. In Proceedings of the 2021 IEEE UFFC Latin America Ultrasonics Symposium (LAUS 2021), Virtual, 4–5 October 2021.
87. Majasan, J.O.; Robinson, J.B.; Owen, R.E.; Maier, M.; Radhakrishnan, A.N.P.; Pham, M.; Tranter, T.G.; Zhang, Y.; Shearing, P.R.; Brett, D.J.L. Recent advances in acoustic diagnostics for electrochemical power systems. *J. Phys. Energy* **2021**, *3*, 032011. [\[CrossRef\]](#)
88. Robinson, J.B.; Owen, R.E.; Kok, M.D.R.; Maier, M.; Majasan, J.; Braglia, M.; Stocker, R.; Amietszajew, T.; Roberts, A.J.; Bhagat, R.; et al. Identifying Defects in Li-Ion Cells Using Ultrasound Acoustic Measurements. *J. Electrochem. Soc.* **2020**, *167*, 120530. [\[CrossRef\]](#)
89. Wu, Y.; Wang, Y.; Yung, W.K.C.; Pecht, M. Ultrasonic health monitoring of lithium-ion batteries. *Electronics* **2019**, *8*, 751. [\[CrossRef\]](#)
90. Wang, Z.; Lu, K.; Chen, X.; Zhen, D.; Gu, F.; Ball, A.D. Rapid State of Health Estimation of Lithium-ion Batteries based on An Active Acoustic Emission Sensing Method. In Proceedings of the 2022 27th International Conference on Automation and Computing (ICAC), Bristol, UK, 1–3 September 2022; pp. 1–6.
91. Zhao, G.; Liu, Y.; Liu, G.; Jiang, S.; Hao, W. State-of-charge and state-of-health estimation for lithium-ion battery using the direct wave signals of guided wave. *J. Energy Storage* **2021**, *39*, 102657. [\[CrossRef\]](#)
92. Robinson, J.B.; Pham, M.; Kok, M.D.R.; Heenan, T.M.M.; Brett, D.J.L.; Shearing, P.R. Examining the Cycling Behaviour of Li-Ion Batteries Using Ultrasonic Time-of-Flight Measurements. *J. Power Sources* **2019**, *444*, 227318. [\[CrossRef\]](#)
93. Popp, H.; Koller, M.; Keller, S.; Glanz, G.; Klambauer, R.; Bergmann, A. State Estimation Approach of Lithium-Ion Batteries by Simplified Ultrasonic Time-of-Flight Measurement. *IEEE Access* **2019**, *7*, 170992–171000. [\[CrossRef\]](#)
94. Davies, G.; Knehr, K.W.; Van Tassell, B.; Hodson, T.; Biswas, S.; Hsieh, A.G.; Steingart, D.A. State of Charge and State of Health Estimation Using Electrochemical Acoustic Time of Flight Analysis. *J. Electrochem. Soc.* **2017**, *164*, A2746–A2755. [\[CrossRef\]](#)
95. Ke, Q.; Jiang, S.; Li, W.; Lin, W.; Li, X.; Huang, H. Potential of ultrasonic time-of-flight and amplitude as the measurement for state of charge and physical changings of lithium-ion batteries. *J. Power Sources* **2022**, *549*, 232031. [\[CrossRef\]](#)
96. Zhang, X.; Cheng, L.; Liu, Y.; Tao, B.; Wang, J.; Liao, R. A review of non-destructive methods for the detection tiny defects within organic insulating materials. *Front. Mater.* **2022**, *9*, 995516. [\[CrossRef\]](#)
97. Cho, H.; Kil, E.; Jang, J.; Kang, J.; Song, I.; Yoo, Y. Air-Coupled Ultrasound Sealing Integrity Inspection Using Leaky Lamb Waves in a Simplified Model of a Lithium-Ion Pouch Battery: Feasibility Study. *Sensors* **2022**, *22*, 6718. [\[CrossRef\]](#)
98. Seco, F.; Jiménez, A.R.; Castillo, M.D.d. Air coupled ultrasonic detection of surface defects in food cans. *Meas. Sci. Technol.* **2006**, *17*, 1409–1416. [\[CrossRef\]](#)
99. Tiiitta, M.; Tiiitta, V.; Gaal, M.; Heikkilä, J.; Lappalainen, R.; Tomppo, L. Air-coupled ultrasound detection of natural defects in wood using ferroelectret and piezoelectric sensors. *Wood Sci. Technol.* **2020**, *54*, 1051–1064. [\[CrossRef\]](#)
100. Li, H.; Zhou, Z. Numerical simulation and experimental study of fluid-solid coupling-based air-coupled ultrasonic detection of stomata defect of lithium-ion battery. *Sensors* **2019**, *19*, 2391. [\[CrossRef\]](#)
101. Chang, J.J.; Zeng, X.F.; Wan, T.L. Real-time measurement of lithium-ion batteries' state-of-charge based on air-coupled ultrasound. *AIP Adv.* **2019**, *9*, 085116. [\[CrossRef\]](#)
102. Cui, Z.; Wang, L.; Li, Q.; Wang, K. A comprehensive review on the state of charge estimation for lithium-ion battery based on neural network. *Int. J. Energy Res.* **2022**, *46*, 5423–5440. [\[CrossRef\]](#)
103. Cui, Z.; Dai, J.; Sun, J.; Li, D.; Wang, L.; Wang, K. Hybrid Methods Using Neural Network and Kalman Filter for the State of Charge Estimation of Lithium-Ion Battery. *Math. Probl. Eng.* **2022**, *2022*, 9616124. [\[CrossRef\]](#)
104. Galiounas, E.; Tranter, T.G.; Owen, R.E.; Robinson, J.B.; Shearing, P.R.; Brett, D.J.L. Battery state-of-charge estimation using machine learning analysis of ultrasonic signatures. *Energy AI* **2022**, *10*, 100188. [\[CrossRef\]](#)
105. Sun, H.; Muralidharan, N.; Amin, R.; Rathod, V.; Ramuhalli, P.; Belharouak, I. Ultrasonic nondestructive diagnosis of lithium-ion batteries with multiple frequencies. *J. Power Sources* **2022**, *549*, 232091. [\[CrossRef\]](#)
106. Huang, M.; Kirkaldy, N.; Zhao, Y.; Patel, Y.; Cegla, F.; Lan, B. Quantitative characterisation of the layered structure within lithium-ion batteries using ultrasonic resonance. *J. Energy Storage* **2022**, *50*, 14. [\[CrossRef\]](#)
107. Gold, L.; Bach, T.; Virsik, W.; Schmitt, A.; Müller, J.; Staab, T.E.M.; Sextl, G. Probing lithium-ion batteries' state-of-charge using ultrasonic transmission—Concept and laboratory testing. *J. Power Sources* **2017**, *343*, 536–544. [\[CrossRef\]](#)

108. Li, X.; Wu, C.; Fu, C.; Zheng, S.; Tian, J. State Characterization of Lithium-Ion Battery Based on Ultrasonic Guided Wave Scanning. *Energies* **2022**, *15*, 6027. [[CrossRef](#)]
109. Hsieh, A.G.; Bhadra, S.; Hertzberg, B.J.; Gjeltema, P.J.; Goy, A.; Fleischer, J.W.; Steingart, D.A. Electrochemical-acoustic time of flight: In operando correlation of physical dynamics with battery charge and health. *Energy Environ. Sci.* **2015**, *8*, 1569–1577. [[CrossRef](#)]
110. Ladpli, P.; Kopsaftopoulos, F.; Chang, F.-K. Estimating State of Charge and Health of Lithium-ion Batteries with Guided Waves Using Built-in Piezoelectric Sensors/Actuators. *J. Power Sources* **2018**, *384*, 342–354. [[CrossRef](#)]
111. Robinson, J.B.; Maier, M.; Alster, G.; Compton, T.; Brett, D.J.L.; Shearing, P.R. Spatially resolved ultrasound diagnostics of Li-ion battery electrodes. *Phys. Chem. Chem. Phys.* **2019**, *21*, 6354–6361. [[CrossRef](#)] [[PubMed](#)]
112. Akbar, K.; Zou, Y.; Awais, Q.; Baig, M.J.A.; Jamil, M. A Machine Learning-Based Robust State of Health (SOH) Prediction Model for Electric Vehicle Batteries. *Electronics* **2022**, *11*, 1216. [[CrossRef](#)]
113. Zappen, H.; Fuchs, G.; Gitis, A.; Sauer, D.U. In-operando impedance spectroscopy and ultrasonic measurements during high-temperature abuse experiments on lithium-ion batteries. *Batteries* **2020**, *6*, 25. [[CrossRef](#)]
114. Siegl, A.; Schweighofer, B.; Bergmann, A.; Wegleiter, H. An Electromagnetic Acoustic Transducer for Generating Acoustic Waves in Lithium-Ion Pouch Cells. In Proceedings of the 2022 IEEE International Instrumentation and Measurement Technology Conference (I2MTC), Ottawa, ON, Canada, 16–19 May 2022.

Disclaimer/Publisher's Note: The statements, opinions and data contained in all publications are solely those of the individual author(s) and contributor(s) and not of MDPI and/or the editor(s). MDPI and/or the editor(s) disclaim responsibility for any injury to people or property resulting from any ideas, methods, instructions or products referred to in the content.